

Coding and Equalization for PPM on Wireless Infrared Channels

David C. M. Lee, *Student Member, IEEE*, and Joseph M. Kahn, *Senior Member, IEEE*

Abstract—We analyze the performance of trellis-coded pulse-position modulation with block decision-feedback equalization (BDFE) and parallel decision-feedback decoding (PDFD) on indoor, wireless infrared channels. We show that the reduced complexities of BDFE and PDFD as compared to maximum-likelihood sequence detection allow for better codes whose increased coding gain more than compensates for the penalty due to suboptimal detection. We quantify these net gains in performance over a range of dispersive channels, indicating where BDFE and PDFD provide the best performance. Finally, we present Monte Carlo simulation results to verify our analysis.

Index Terms—Decision-feedback equalizers, maximum-likelihood decoding, optical communication, pulse-position modulation, trellis-coded modulation.

I. INTRODUCTION

INFRARED (IR) radiation using intensity modulation with direct detection is a viable medium for short-range, indoor, wireless communication [1]–[3]. IR offers an enormous unregulated bandwidth and is free from interference between links operating in different rooms. The spatial diversity of large-area photodetectors prevents multipath fading, but diffuse links, which provide ease of use and robustness against shadowing, are subject to multipath dispersion that can severely degrade system performance above 10 Mbaud [3].

Pulse-position modulation (PPM) offers high average-power efficiency, but due to its poor bandwidth efficiency, it is more susceptible to multipath-induced intersymbol interference (ISI) than simple on-off keying (OOK). Barry [4] discussed maximum-likelihood sequence detection (MLSD) and various suboptimal equalizers for PPM, but even with optimal MLSD, uncoded PPM suffers larger ISI penalties than OOK [5]. This led the authors to apply trellis-coded modulation principles to PPM.

The authors found that trellis-coded PPM (TC-PPM) is very effective in mitigating the effects of ISI [6], but the high computational demands of MLSD of the combined code and ISI states preclude the use of high-constraint-length codes or op-

eration under severe channel conditions. Suboptimal, reduced-complexity decoding techniques allow for better codes at the cost of a penalty due to the suboptimal decoding. When the gain due to a better code is greater than the penalty due to suboptimal decoding, there is a net gain for the same computational complexity. There are a variety of suboptimal techniques, such as delayed decision-feedback sequence estimation, parallel decision-feedback decoding (PDFD), precoding, decision-feedback equalization (DFE), and linear equalization (LE). These techniques are listed roughly in order of decreasing decoding complexity, although precoding requires a reverse channel and a more complex transmitter. Park [7] performed limited simulations of the performance of TC-PPM using PDFD, partial-response precoding with PDFD, block DFE (BDFE), and LE. In this paper, we analyze the performance of PDFD and BDFE. We will show that BDFE and PDFD provide net gains over MLSD for the same complexity over a wide range of multipath ISI channels. We present results on these net performance gains, indicating under which conditions each technique provides the best performance. Finally, we provide Monte Carlo simulations to verify the analysis and to quantify the effects of error propagation in BDFE.

II. CHANNEL AND NOISE MODELS

Practical wireless infrared links use intensity modulation and direct detection (IM/DD). The channel model for an IM/DD link is given by

$$Z(t) = RX(t) \otimes h(t) + N(t), \quad (1)$$

The received photocurrent $Z(t)$ is the convolution of the transmitted optical power $X(t)$ with a channel impulse response $h(t)$ (fixed for a given configuration of transmitter, receiver, and intervening reflectors), scaled by the photodetector responsivity R , plus an additive noise $N(t)$, which is usually modeled as white, Gaussian, and independent of $X(t)$ [3].

The average transmitted optical power is given by

$$P_t = \lim_{T \rightarrow \infty} \frac{1}{2T} \int_{-T}^T X(t) dt. \quad (2)$$

For the purpose of computing the average power P_t required to achieve a certain bit rate R_b and bit-error probability P_e , only two key parameters are needed to characterize multipath IR channels: dc gain H_0 , given by $H_0 = \int_{-\infty}^{\infty} h(t) dt$, and root-mean-square delay spread D [8]. These parameters correspond, respectively, to the optical path loss and multipath power requirement. We define the normalized power

Paper approved by J. J. O'Reilly, the Editor for Optical Communications of the IEEE Communications Society. Manuscript received February 8, 1998; revised August 4, 1998. This work was supported by National Science Foundation Grant ECS-9710065, LG Electronics, Hewlett-Packard, and the University of California MICRO Program.

D. C. M. Lee was with the Department of Electrical Engineering and Computer Sciences, University of California, Berkeley, CA 94720 USA. He is now with Calimetrics, Inc., Alameda, CA 94501 USA (e-mail: dcleee@EECS.Berkeley.edu).

J. M. Kahn is with the Department of Electrical Engineering and Computer Sciences, University of California, Berkeley, CA 94720 USA (e-mail: jmk@EECS.Berkeley.edu).

Publisher Item Identifier S 0090-6778(99)01928-5.

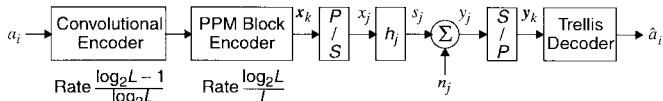


Fig. 1. Discrete-time trellis-coded L -PPM system block diagram.

requirement to be the optical power P_t required for a given modulation scheme on the channel $h(t)$ divided by the power required for on-off keying on the ideal channel $\delta(t)$ with the same R_b , P_e , and H_0 . We further define the normalized delay spread to be $D_T = DR_b$.

We use the ceiling-bounce functional model for the channel impulse response

$$h(t) = H_0 6a^6 (t+a)^{-7} u(t) \quad (3)$$

where the delay spread $D = 0.0906a$. The use of this model provides a simple, fairly accurate, reproducible method of evaluating the performance of PPM on multipath channels [8].

The average received power is $P = H_0 P_t$. To facilitate the comparison of optical average-power efficiency in later sections, we define the electrical signal-to-noise ratio (SNR) to be $R^2 P^2 / (R_b N_0)$, where N_0 is the one-sided noise power spectral density. For L -PPM, it is equal to $1/L$ times the usual definition of SNR (E_b/N_0).

III. SYSTEM DESCRIPTION

Fig. 1 shows a discrete-time block diagram of a trellis-coded L -PPM system. Information bits a_i with rate R_b (b/s) enter a rate- $(\log_2 L - 1)/\log_2 L$ convolutional encoder concatenated with a rate- $\log_2 L/L$ PPM block encoder, producing length- L vectors, or PPM symbols, $\mathbf{x}_k = (x_{kL}, \dots, x_{kL+L-1})^T$ having unit Hamming weight. The position of the nonzero term, or pulse, in each symbol encodes the $\log_2 L$ input bits. The sequence \mathbf{x}_k passes through the causal, minimum-phase, discrete-equivalent impulse response h_j representing the combination of transmitter filter, multipath channel, and whitened-matched filter (WMF) [9]. We normalize h_j according to $\sum h_j = LPR/\sqrt{N_0}$, the peak received photocurrent divided by the square root of the noise PSD. The noise samples n_j are white and Gaussian with zero mean and unit variance. The received samples y_j are given by

$$y_j = h_j \otimes x_j + n_j = s_j + n_j \quad (4)$$

where s_j denotes the signal component. These samples are grouped into length- L blocks \mathbf{y}_k and sent to the trellis decoder. Fig. 2(a) shows the equivalent vector channel model, which is given by

$$\mathbf{y}_k = \mathbf{H}_k \otimes \mathbf{x}_k + \mathbf{n}_k = \mathbf{s}_k + \mathbf{n}_k \quad (5)$$

where the channel impulse response is a Toeplitz sequence \mathbf{H}_k , with $[\mathbf{H}_k]_{ij} = h_{kL+i-j}$, and $\mathbf{H}(z) = \sum \mathbf{H}_k z^{-k}$.

Fig. 2(b) shows the MLSD trellis decoder, which uses a symbol-rate Viterbi algorithm with a superstate trellis consisting of combined code and ISI states. It chooses an estimate $\hat{\mathbf{x}}_k$ of \mathbf{x}_k that minimizes the total path metric, which is the sum of per-block branch metrics $\|\mathbf{y}_k - \mathbf{H}_k \otimes \hat{\mathbf{x}}_k\|^2$, where $\|\mathbf{y}_k\|^2 = \sum_{j=0}^{L-1} |y_{kL+j}|^2$ denotes the squared Euclidean norm.

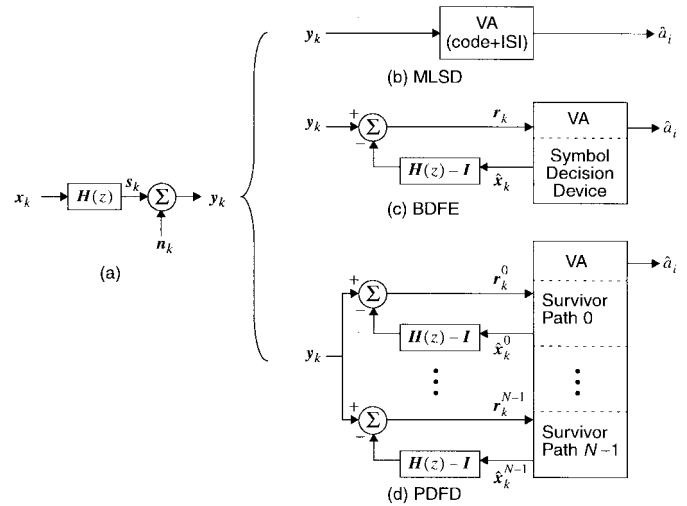


Fig. 2. (a) Equivalent vector channel of TC-PPM system. (b) Block diagram of the MLSD trellis decoder, which uses a symbol-rate Viterbi algorithm (VA) with combined code and ISI states. (c) Block diagram of the BDFE trellis decoder, which uses a feedback filter and a symbol-rate VA with code states only. Feedback symbol decisions are the zero-delay trellis decisions. (d) Block diagram of the PDFD trellis decoder, which uses parallel feedback filters and a symbol-rate VA with code states only. There is a separate feedback filter for each code-state survivor path.

Fig. 2(c) shows the trellis decoder for zero-forcing BDFE (ZF-BDFE). The performance of minimum mean-squared-error (MMSE) DFE's is generally superior to that of ZF-DFE's, but at high SNR their performance is virtually the same [10]. In the case of PPM, the analysis of ZF-BDFE is much easier than that of MMSE-BDFE [11], so we will consider only ZF-BDFE in this paper. The trellis decoder replaces the superstate Viterbi decoder with a feedback filter and a symbol-rate Viterbi decoder with code states only. The feedback block decisions $\hat{\mathbf{x}}_k$ are the zero-delay trellis decisions from the Viterbi decoder. Under the ZF criterion, the feedback filter removes all of the ISI, but retains the intrasymbol interference, which the Viterbi decoder uses in decoding the trellis code. The equalized signal sent to the Viterbi decoder is given by

$$\mathbf{r}_k = \mathbf{H}_0 \mathbf{x}_k + \sum_{j=1}^K \mathbf{H}_j (\mathbf{x}_{k-j} - \hat{\mathbf{x}}_{k-j}) + \mathbf{n}_k \quad (6)$$

where K , the index of the last nonzero term in \mathbf{H}_k , represents the channel length measured in symbols. The symbol-rate Viterbi decoder uses a per-symbol branch metric $\|\mathbf{r}_k - \mathbf{H}_0 \hat{\mathbf{x}}_k\|^2$.

Fig. 2(d) shows the PDFD trellis decoder, which performs ZF-BDFE on each survivor path in the trellis based on the history of that path, where the Viterbi decoder trellis once again only has code states. Given a trellis state $i \in \{0, \dots, N-1\}$, $N = 2^\nu$, with survivor path $\hat{\mathbf{x}}_k^i$, the equalized signal is given by

$$\mathbf{r}_k^i = \mathbf{H}_0 \mathbf{x}_k + \sum_{j=1}^K \mathbf{H}_j (\mathbf{x}_{k-j} - \hat{\mathbf{x}}_{k-j}^i) + \mathbf{n}_k. \quad (7)$$

The Viterbi decoder uses a per-symbol branch metric $\|\mathbf{r}_k - \mathbf{H}_0 \hat{\mathbf{x}}_k^i\|^2$.

IV. ERROR PROBABILITY ANALYSIS

Let $\mathbf{e}_k = \mathbf{x}_k - \mathbf{x}'_k$ be a nonzero error event $\{e\}$ starting at time zero from the transmitted sequence \mathbf{x}_k . For MLSD, the squared Euclidean distance between \mathbf{x}_k and \mathbf{x}'_k is given by

$$d_{M,\{e\}}^2 = \sum_{k=0}^{\infty} \|\mathbf{H}_k \otimes \mathbf{e}_k\|^2. \quad (8)$$

For BDFE, we use the standard assumption in DFE analysis that all previous symbols have been detected correctly and ignore symbol-to-symbol error propagation [10]. If we assume perfect decisions, $\hat{\mathbf{x}}_k = \mathbf{x}_k$, then the squared Euclidean distance between \mathbf{x}_k and \mathbf{x}'_k is given by

$$d_{B,\{e\}}^2 = \sum_{k=0}^{\infty} \|\mathbf{H}_0 \mathbf{e}_k\|^2. \quad (9)$$

We refer to this as ideal BDFE.

For PDFD, we assume that previous symbols have been detected correctly. The squared Euclidean distance from \mathbf{x}_k to \mathbf{x}'_k is given by

$$d_{P,\{e\}}^2 = \sum_{k=0}^{\infty} \left\| \mathbf{H}_0 \mathbf{e}_k - \sum_{j=1}^K \mathbf{H}_j \mathbf{e}_{k-j} \right\|^2. \quad (10)$$

In each case, the pairwise probability of error is given by

$$P_{X,\{e\}} = Q\left(\frac{d_{X,\{e\}}}{2}\right), \quad X = M, B, P. \quad (11)$$

If we sum over all possible error events $\{e\}$ to form a union bound, the probability of bit error for the transmitted sequence \mathbf{x}_k is bounded from above by

$$P_X[\text{bit error} \mid \text{transmit}\{\mathbf{x}_k\}] \leq \sum_{\{e\}} m_{X,\{e\}} Q\left(\frac{d_{X,\{e\}}}{2}\right) \quad (12)$$

where $m_{X,\{e\}}$ is the number of bit errors associated with $\{e\}$. If we choose the error event with the smallest distance, then the corresponding term in (12) forms a minimum-distance lower bound for the probability of bit error.

Since the uniform error property does not hold, in order to calculate bounds on the bit-error probability P_e for a random information bit sequence (i.i.d., $P[\text{bit } 0] = P[\text{bit } 1] = 1/2$), we must average over all possible transmitted sequences, which is not feasible [12].

One alternative is to find best- and worst-case transmitted paths. Note that the feedback filter destroys a different amount of energy for different symbols. For symbol $l \in \{0, \dots, L-1\}$, the fraction of symbol energy retained is $\sum_{j=0}^{L-1-l} h_j$, with the remainder being destroyed by the feedback filter (assuming correct decisions) as ISI. Thus the best- and worst-case transmitted sequences are the all-0's and all- $(L-1)$'s sequences, respectively. We would expect that the all- $(L-1)$'s transmitted sequence will result in one of the highest bit-error probabilities, certainly above the average, and vice-versa for the all-0's sequence.

It turns out, however, that the distance spectra and corresponding bit-error probabilities of most sequences are similar,

TABLE I
CHANNEL MEMORY FOR VARIOUS NORMALIZED DELAY SPREADS. THE CHANNELS HAVE INFINITE IMPULSE RESPONSES, BUT HAVE BEEN TRUNCATED TO REMOVE TERMS LESS THAN 0.01 TIMES THE LARGEST TERM. THE LOSS IN ENERGY DUE TO TRUNCATION IS NEGLIGIBLE

Normalized Delay Spread D_T	Channel Memory K for TC 8-PPM	Channel Memory K for TC 16-PPM
0.2	1	1
0.3	2	2
0.4	3	2
0.7	4	3
0.9	5	–
1.0	–	4

so averaging the bit-error probabilities over, say, 20 randomly chosen transmitted sequences (i.i.d., equiprobable information bits; initial trellis state uniformly distributed) yields very accurate lower and upper bounds. In the next section, we will provide Monte Carlo simulation results to verify this. We also provide simulation results on the effect of decision errors in BDFE.

Since MLSD is optimal, the average probability of bit error for MLSD should be less than those for PDFD and BDFE. Since PDFD guarantees correct feedback for the transmitted path, its performance should also be better than BDFE. However, ideal BDFE uses side information (perfect decisions), so it is possible for it to have better performance than MLSD for coded systems [13]. Moreover, for a given transmitted path, the minimum distance for MLSD may be lower than those for PDFD and ideal BDFE. For a given path, the minimum-distance error events for the three techniques usually are the same error event, but may sometimes be different.

V. PERFORMANCE ON MULTIPATH ISI CHANNELS

We evaluated the performance of TC-PPM with BDFE and PDFD over a range of multipath ISI channels. We used codes published in [6], which were the best codes found for MLSD distance spectra. The distance spectra for BDFE and PDFD are slightly different, so it is conceivable that other codes would perform better for these suboptimal techniques. However, MLSD performance provides a lower bound on the power requirement of all suboptimal techniques. We will show that the BDFE and PDFD penalties with respect to MLSD are very small, so a search for better codes using these distance spectra would provide at best only marginal improvement in performance.

The number of states in the Viterbi decoder provides a simple, fairly accurate measure of the implementation complexity of the Viterbi algorithm. For MLSD, the number of combined code and ISI states is $2^\nu (L/2)^K$. Table I lists the channel memory K for different delay spreads D_T for TC 8-PPM and TC 16-PPM.

In BDFE and PDFD, the feedback filter(s) obviate the need for ISI trellis states, reducing the number of states in the Viterbi algorithm to 2^ν . For $L = 8$ -PPM (or 16-PPM), with BDFE, each ISI symbol that the feedback filter removes allows for a

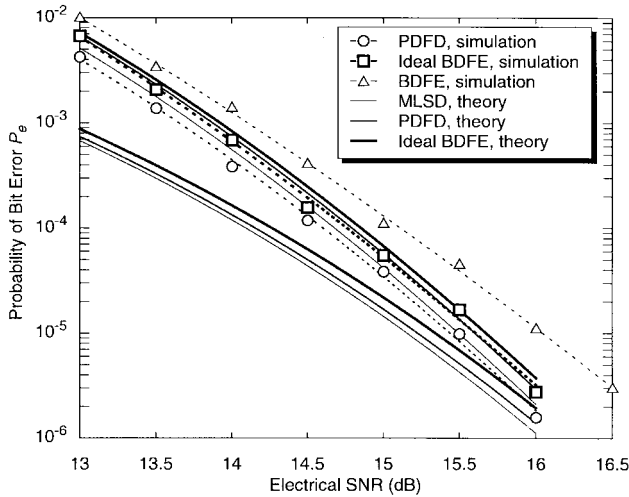


Fig. 3. Performance of TC 8-PPM, $\nu = 6$, with MLSD, PDFD, ideal BDFE, and BDFE, on $D_T = 0.9$ channel. Simulated PDFD and ideal BDFE curves lie between their respective minimum-distance and union-bound curves.

$\Delta\nu = 2$ (or 3) increase in the code constraint length for BDFE. In PDFD, because there is a feedback filter for each code-state survivor path, the complexity is slightly higher than that of BDFE. More precisely, in BDFE, extending each of the 2^ν survivor paths requires L additions, whereas in PDFD, extending each survivor path requires approximately L^2K additions [14]. For moderate to large ν , survivor-path-extension computations dominate over all other computations, so that PDFD requires roughly a factor LK greater computational complexity than BDFE, which corresponds to $\Delta\nu = \log_2(LK)$ difference in code constraint length for the same complexity. However, both techniques require extensive memory storage, approximately $5(\nu + K)(\log_2 L - 1)$ bits, for each survivor path. Extending each survivor path thus requires substantial memory transfer, which, depending on the ratio of addition-to-memory-transfer clock cycles, can have a significant impact on overall decoding speed. In our C++ simulations, we found that PDFD was two to three times slower than BDFE, which translates into approximately a unit constraint-length difference.

Fig. 3 shows the theoretical and simulated performance of the various decoding techniques for TC 8-PPM with $\nu = 6$ on a severe ISI channel, $D_T = 0.9$. The theoretical curves are the minimum-distance and union-bound curves averaged over 20 randomly chosen transmitted paths. The simulation curves for PDFD and ideal BDFE (perfect feedback decisions) both lie between their respective lower and upper bounds, which verifies the accuracy of the theory. The simulations show that decision errors in BDFE cause a 0.43 dB penalty with respect to ideal BDFE at $P_e = 10^{-5}$, which is significant but not excessive.

Fig. 4 shows the theoretical performance of MLSD of TC 8-PPM with $\nu = 4$ and 10, and MLSD of TC 16-PPM with $\nu = 4$ and 9, at $P_e = 10^{-5}$ over a range of channels. These curves are minimum-distance lower bounds averaged over 50 randomly chosen transmitted paths. The performance of MLSD provides a baseline from which to compare that of PDFD and BDFE.

Using these same paths, we evaluated the performance of PDFD and BDFE. For each constraint length $\nu = 4$ to 10 for

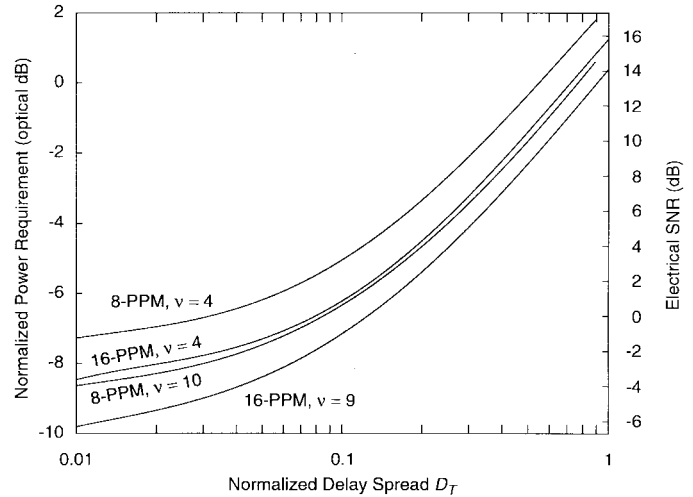


Fig. 4. Normalized power requirement versus normalized delay spread for MLSD of TC 8-PPM with $\nu = 4$ and 10, and TC 16-PPM with $\nu = 4$ and 9. All curves are minimum-distance lower bounds averaged over 50 randomly chosen transmitted paths. The vertical axis shows the SNR required to achieve $P_e = 10^{-5}$. The 0-dB optical-power reference level is on-off keying on the ideal channel.

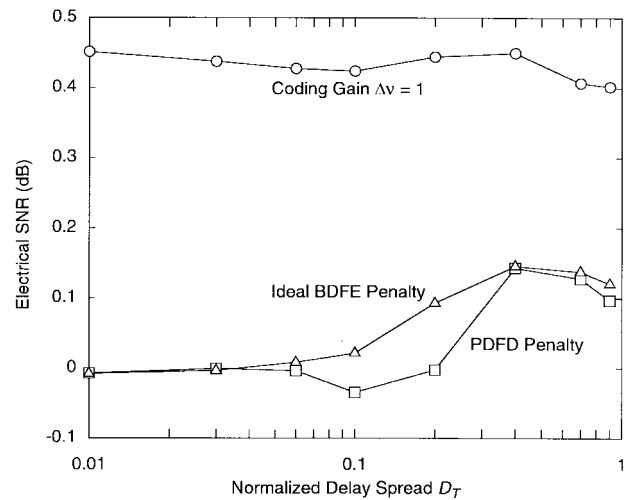


Fig. 5. Average suboptimal-decoding SNR penalties of PDFD and ideal BDFE with respect to MLSD for TC 8-PPM for $\nu = 4$ to 10 at $P_e = 10^{-5}$ over a range of channels. These penalties are computed from the minimum-distance lower bounds. Also shown are average coding gains due to a unit increase in the code constraint length ν .

TC 8-PPM, and $\nu = 4$ to 9 for TC 16-PPM, we calculated the electrical SNR required for each technique at $P_e = 10^{-5}$, and the resulting PDFD and ideal BDFE SNR penalties with respect to MLSD. We then averaged these penalties over the different constraint lengths. We also calculated the average coding gain as ν increased from 4 to 10 or 9, for TC 8-PPM and TC 16-PPM, respectively.

Figs. 5 and 6 show these average theoretical suboptimal-decoding penalties for PDFD and ideal BDFE for TC 8-PPM and TC 16-PPM, respectively, at $P_e = 10^{-5}$ over a range of channels. The figures also show the average coding gains for a unit increase in the code constraint length. These coding gains range from 0.45 dB to 0.40 dB for TC 8-PPM, and from 0.54 dB to 0.34 dB for TC 16-PPM. By contrast, the

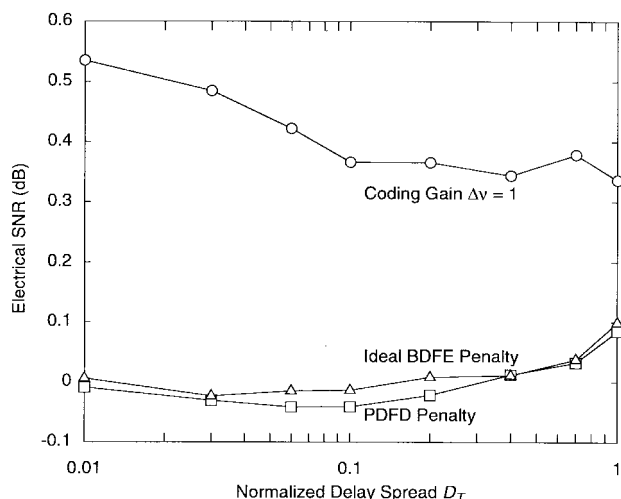


Fig. 6. Average suboptimal-decoding SNR penalties of PDFD and ideal BDFE with respect to MLSD for TC 16-PPM for $\nu = 4$ to 9 at $P_e = 10^{-5}$ over a range of channels. These penalties are computed from the minimum-distance lower bounds. Also shown are the average coding gains due to a unit increase in the code constraint length ν .

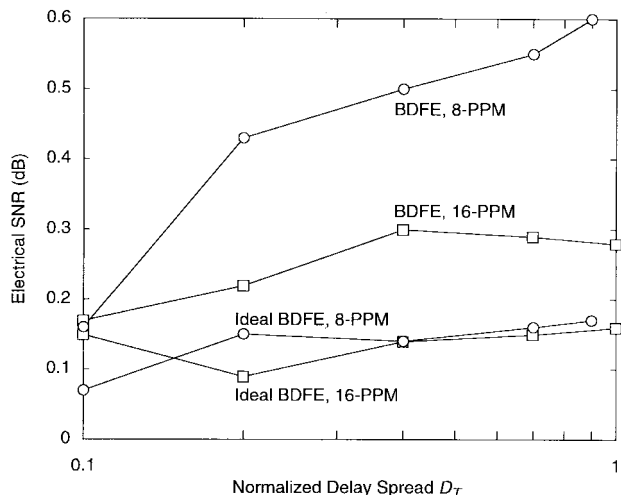


Fig. 7. Simulation results on the difference in performance of BDFE and ideal BDFE as compared to PDFD for TC 8-PPM and TC 16-PPM at $P_e = 10^{-5}$ over a range of channels.

penalties over the entire range of channels are much lower than these coding gains, which indicates that one can always obtain a net gain, for the same complexity, by using PDFD or ideal BDFE instead of MLSD. This net gain can range from half a decibel to a few decibels as the delay spread increases. Indeed, the penalties are so small that the theoretical bounds, which accurately predict the performances within a fraction of a decibel, can only provide an order-of-magnitude estimate of these differences in performance. For TC 8-PPM on channels with $D_T < 0.1$, these penalties are negligible; on channels with $D_T > 0.1$, the penalties are around 0.15 dB. For TC 16-PPM on all channels, the penalties are under 0.1 dB.

In order to determine more precisely the difference in performance between PDFD and ideal BDFE, as well as to determine the impact of decision errors in BDFE, we conducted extensive simulations. Fig. 7 shows simulation results of the SNR penalties of BDFE and ideal BDFE with respect

to PDFD for $D_T > 0.1$ at $P_e = 10^{-5}$. Ideal BDFE for both TC 8-PPM and TC 16-PPM performs about 0.15 dB worse than PDFD. For TC 16-PPM, decision errors in BDFE cause an additional penalty of up to 0.15 dB, for a total penalty of about 0.2 to 0.3 dB, which is less than the coding gain of 0.34 to 0.54 dB, so that BDFE gives the best overall performance for the same complexity. For TC 8-PPM, however, decision errors in BDFE cause substantially larger penalties, from 0.1 to 0.43 dB, for total penalties of 0.2 to 0.6 dB. In particular, for $D_T > 0.2$, the difference in performance between BDFE and PDFD is larger than the coding gain of 0.4 dB, so that PDFD gives the best overall performance in that region.

VI. CONCLUSION

We have analyzed the performance of TC-PPM with BDFE and PDFD. We also investigated the effect of decision errors in BDFE through simulations. We quantified the computational complexities of BDFE, PDFD, and MLSD. We then showed that the reduced complexities of BDFE and PDFD as compared to MLSD allow for better codes whose increased coding gains are greater than the penalties due to suboptimal detection, thus providing net gains in performance for the same complexity. We quantified these net gains over a wide range of multipath channels. For TC 16-PPM, BDFE provides the best performance. For TC 8-PPM, BDFE provides the best performance for normalized delay spreads $D_T < 0.2$, but because of significant penalties due to decision errors in BDFE, PDFD provides the best performance for $D_T > 0.2$.

REFERENCES

- [1] F. R. Gfeller and U. H. Bapst, "Wireless in-house data communication via diffuse infrared radiation," *Proc. IEEE*, vol. 67, pp. 1474–1486, Nov. 1979.
- [2] J. R. Barry, *Wireless Infrared Communications*. Boston: Kluwer, 1994.
- [3] J. M. Kahn and J. R. Barry, "Wireless infrared communications," *Proc. IEEE*, vol. 85, pp. 265–98, Feb. 1997.
- [4] J. R. Barry, "Sequence detection and equalization for pulse-position modulation," in *Proc. IEEE Int. Conf. Communications (ICC'94)*, New Orleans, LA, May 1–5, 1994, pp. 1561–1565.
- [5] M. D. Audeh, J. M. Kahn, and J. R. Barry, "Performance of pulse-position modulation on measured nondirected indoor infrared channels," *IEEE Trans. Commun.*, vol. 44, pp. 654–659, June 1996.
- [6] D. C. Lee, J. M. Kahn, and M. D. Audeh, "Trellis-coded pulse-position modulation for wireless indoor infrared communications," *IEEE Trans. Commun.*, vol. 45, pp. 1080–1087, Sept. 1997.
- [7] H. Park, "Coded modulation and equalization for wireless infrared communications," Ph.D. dissertation, Georgia Inst. Technol., 1997.
- [8] J. B. Carruthers and J. M. Kahn, "Modeling of nondirected wireless infrared channels," *IEEE Trans. Commun.*, vol. 45, pp. 1260–1268, Oct. 1997.
- [9] G. D. Forney, "Maximum-likelihood sequence estimation of digital sequences in the presence of intersymbol interference," *IEEE Trans. Inform. Theory*, vol. IT-18, pp. 363–378, May 1972.
- [10] C. A. Belfiore and J. H. Park Jr., "Decision feedback equalization," *Proc. IEEE*, vol. 67, pp. 1143–1156, Aug. 1979.
- [11] M. D. Audeh, J. M. Kahn, and J. R. Barry, "Decision-feedback equalization of pulse-position modulation on measured indoor infrared channels," in *Proc. IEEE Int. Conf. Communications (ICC'96)*, Dallas, TX, June 23–27, 1996, vol. 2, pp. 1220–1226.
- [12] S. Benedetto, M. A. Marsan, G. Albertengo, and E. Giachin, "Combined coding and modulation: Theory and applications," *IEEE Trans. Inform. Theory*, vol. IT-34, pp. 223–236, Mar. 1988.
- [13] M. V. Eyuboglu and S. U. H. Qureshi, "Reduced-state sequence estimation for coded modulation on intersymbol interference channels," *IEEE J. Select. Areas Commun.*, vol. 7, pp. 989–995, Aug. 1989.
- [14] D. C. Lee, "Power-efficient coded modulation for wireless infrared communication," Ph.D. Dissertation, Univ. California, Berkeley, 1998.



David C. M. Lee (S'88) received the B.Sc. Honors degree in mathematics and the B.E. degree in electrical engineering from the University of Saskatchewan, Saskatoon, Canada, in 1993. He received the Ph.D. degree in electrical engineering from the University of California, Berkeley, in 1998. His Ph.D. dissertation was entitled "Power-Efficient Coded Modulation for Wireless Infrared Communication."

Currently he is working as a Senior Engineer at Calimetrics, Inc., Alameda, CA, developing multi-level optical data storage. His interests include optical communication, optical data storage, wireless communication, coding, equalization, and multiuser detection.

Dr. Lee's doctoral studies were supported by an Office of Naval Research Graduate Fellowship and a Natural Sciences and Engineering Research Council of Canada Scholarship.



Joseph M. Kahn (M'87-SM'98) received the A.B., M.A., and Ph.D. degrees in physics from the University of California, Berkeley, in 1981, 1983, and 1986, respectively. His doctoral research involved infrared spectroscopy of hydrogen-related impurity complexes in semiconductors.

He is a Professor and Vice Chairman in the Department of Electrical Engineering and Computer Sciences at the University of California, Berkeley. From 1987 to 1990 he was a Member of Technical Staff in the Lightwave Communications Research Department of AT&T Bell Laboratories, where he performed research on multi-gigabit-per-second coherent optical fiber transmission systems and related device and subsystem technologies. He joined the faculty of U.C. Berkeley in 1990. His current research addresses several areas of communications, including infrared and radio wireless communications, source and channel coding techniques, and optical fiber communications.

Dr. Kahn received the National Science Foundation Presidential Young Investigator Award in 1991. He is a member of the IEEE Communications Society and the IEEE Lasers and Electro-Optics Society. He is serving currently as a Technical Editor of *IEEE Personal Communications Magazine*.